Nitrous oxide emissions are enhanced in a warmer and wetter world

Timothy J. Griffis[a,1], Zichong Chen[a], John M. Baker[a,b], Jeffrey D. Wood[a,c], Dylan B. Millet[a], Xuhui Lee[d,e], Rodney T. Venterea[a,b], and Peter A. Turner[a,f]

[a]Department of Soil, Water, and Climate, University of Minnesota-Twin Cities, St. Paul, MN 55108; [b]Agricultural Research Service, US Department of Agriculture, St. Paul, MN 55108; [c]School of Natural Resources, University of Missouri, Columbia, MO 65211; [d]School of Forestry and Environmental Studies, Yale University, New Haven, CT 06511; [e]Yale-NUIST Center on Atmospheric Environment, Nanjing University of Information, Science and Technology, Nanjing 210044, China; and [f]Department of Global Ecology, Carnegie Institution for Science, Stanford, CA 94305

Edited by Keith A. Smith, University of Edinburgh, Edinburgh, United Kingdom, and accepted by Editorial Board Member Hans J. Schellnhuber September 10, 2017 (received for review March 19, 2017)

Nitrous oxide (N_2O) has a global warming potential that is 300 times that of carbon dioxide on a 100-y timescale, and is of major importance for stratospheric ozone depletion. The climate sensitivity of N_2O emissions is poorly known, which makes it difficult to project how changing fertilizer use and climate will impact radiative forcing and the ozone layer. Analysis of 6 y of hourly N_2O mixing ratios from a very tall tower within the US Corn Belt—one of the most intensive agricultural regions of the world—combined with inverse modeling, shows large interannual variability in N_2O emissions (316 Gg N_2O-N·y^{-1} to 585 Gg N_2O-N·y^{-1}). This implies that the regional emission factor is highly sensitive to climate. In the warmest year and spring (2012) of the observational period, the emission factor was 7.5%, nearly double that of previous reports. Indirect emissions associated with runoff and leaching dominated the interannual variability of total emissions. Under current trends in climate and anthropogenic N use, we project a strong positive feedback to warmer and wetter conditions and unabated growth of regional N_2O emissions that will exceed 600 Gg N_2O-N·y^{-1}, on average, by 2050. This increasing emission trend in the US Corn Belt may represent a harbinger of intensifying N_2O emissions from other agricultural regions. Such feedbacks will pose a major challenge to the Paris Agreement, which requires large N_2O emission mitigation efforts to achieve its goals.

nitrous oxide emissions | agriculture | climate change | synthetic nitrogen | atmospheric inversion

Global demand for synthetic nitrogen (N) fertilizer is projected to exceed 119 Tg (1 Tg = 10^{12} g) N in 2018—a 29% increase since 2008 (1). The current trajectory of N fertilizer demand is exceeding some of the most aggressive forecasts (2). Globally, about 4% of the anthropogenic N in agricultural systems is returned to the atmosphere as nitrous oxide (N_2O) (3)—a potent greenhouse gas (4) and the predominant stratospheric ozone-depleting emission (5). Growing population and demand for food, fiber, and biofuel are accelerating the use of synthetic N and N_2O emissions (6, 7).

In recent decades (1987–2012), N fertilizer use within the US Corn Belt has averaged (mean ± 1 SD) 6.2 ± 0.9 Tg N (8), with a significant increasing trend (+0.08 Tg N·y^{-1}, $P < 0.01$) (*SI Appendix*, Fig. S1). With each passing decade, an additional 1 Tg of new synthetic N is added to this intensively managed region. Biological nitrogen fixation has also increased over the past three decades as a result of increasing soybean production (*SI Appendix*, Fig. S1). This implies that N_2O emissions should be increasing by at least 4 Gg N_2O-N·y^{-1}. The production and application of organic N (as manure) in the Corn Belt has been relatively stable at 2.0 ± 0.15 Tg N over the same period, but has been increasing globally along with animal protein consumption, thereby enhancing N_2O emissions (9). However, the interannual variability of N_2O emissions from the major agricultural regions of the world and the extent to which climate variations modulate emissions remains poorly known (10, 11).

Climate models and observations indicate that convective precipitation is enhanced in a warmer world, with wet areas becoming wetter (12). These warmer and wetter conditions are expected to enhance N_2O production via (de)nitrification (13). Within the US Corn Belt, air temperature and precipitation have increased over the period 1895–2015 by 0.67 °C per century and 75 mm per century, respectively (14). We posit that increasing trends in anthropogenic N and warmer and wetter conditions in agricultural regions are enhancing N_2O emissions and that these trends will be amplified via positive feedback to climate change.

Here, we analyze high-precision hourly N_2O mixing ratios measured at a tall tower in Minnesota (100 m above ground level) from April 2010 to April 2016 (*SI Appendix*, Figs. S2 and S3) to examine the sensitivity of N_2O emissions to weather and climate phenomena within the US Corn Belt. We use Bayesian inverse modeling to constrain the total regional N_2O emissions for each year and to partition the emissions into direct and indirect components (15), defined here as emissions from cropped and grazed lands and emissions occurring off-site, respectively. Indirect emissions result from leaching and runoff of fertilizer and manure N as well as deposition of reactive N (16) and have been shown to be significantly larger than previously reported for this region (15, 17). These improved constraints on N_2O emissions were then used to optimize the Community Land Model to evaluate climate feedbacks on N_2O emissions from present to the year 2050.

Significance

N_2O has 300 times the global warming potential of CO_2 on a 100-y timescale, and is of major importance for stratospheric ozone depletion. The climate sensitivity of N_2O emissions is poorly known, which makes it difficult to project how changing fertilizer use and climate will impact radiative forcing and the ozone layer. Here, atmospheric inverse analyses reveal that direct and indirect N_2O emissions from the US Corn Belt are highly sensitive to perturbations in temperature and precipitation. We combine top-down constraints on these emissions with a land surface model to evaluate the climate feedback on N_2O emissions. Our results show that, as the world becomes warmer and wetter, such feedbacks will pose a major challenge to N_2O mitigation efforts.

Author contributions: T.J.G. and Z.C. designed research; T.J.G. and Z.C. performed research; J.M.B., J.D.W., D.B.M., X.L., R.T.V., and P.A.T. contributed new reagents/analytic tools; T.J.G. and Z.C. analyzed data; and T.J.G., Z.C., J.M.B., J.D.W., D.B.M., X.L., R.T.V., and P.A.T. wrote the paper.

The authors declare no conflict of interest.

This article is a PNAS Direct Submission. K.A.S. is a guest editor invited by the Editorial Board.

[1]To whom correspondence should be addressed. Email: timgriffis@umn.edu.

This article contains supporting information online at www.pnas.org/lookup/suppl/doi:10.1073/pnas.1704552114/-/DCSupplemental.

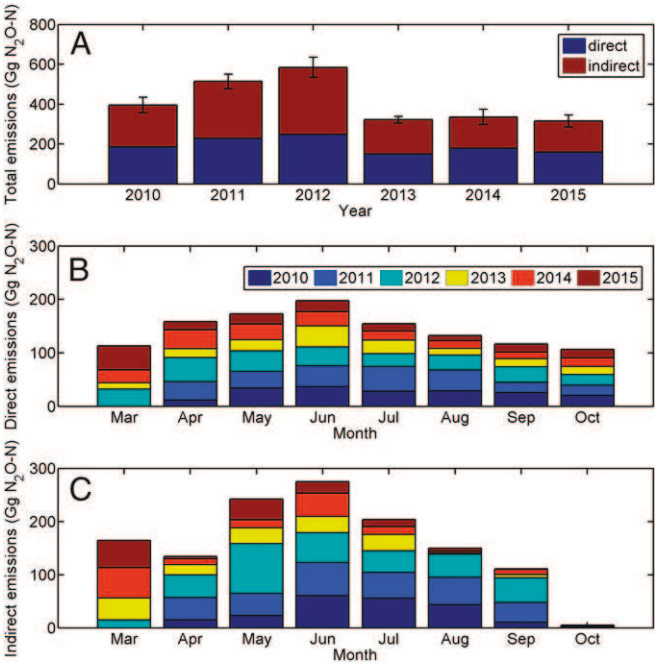

Fig. 1. Interannual variability of N_2O emissions from the US Corn Belt based on Bayesian atmospheric inverse analyses. (*A*) Total emissions from 2010 to 2015. (*B*) Direct emissions. (*C*) Indirect emissions. The error bars in *A* represent the sensitivity of the total Bayesian inversion estimate to model assumptions related to background and tall tower concentration uncertainty, data quality control, and model transport processes.

Results and Discussion

Atmospheric inversions (15) reveal that the interannual variability of N_2O emissions is large, varying from 316 Gg N_2O-N·y^{-1} to 585 Gg N_2O-N·y^{-1} (mean = 411 ± 113 Gg N_2O-N·y^{-1}) (Fig. 1). Further, direct (192 ± 39 Gg N_2O-N·y^{-1}) and indirect (220 ± 75 Gg N_2O-N·y^{-1}) emissions are similar on average (15, 17), but indirect emissions contribute more to the interannual variability of the regional N_2O budget. Indeed, the interannual variability of nitrate export from the Mississippi River has also been shown to be large, varying from 0.02 T nitrate N to 0.08 Tg nitrate N, and is highly sensitive to variations in winter and spring precipitation (18). The export of nitrate from runoff and leaching is known to be an important control on dissolved N_2O concentrations and fluxes from riverine systems within the region (17, 19), and we expect increases in winter and spring precipitation to amplify the indirect emissions.

The large interannual variability in the N_2O budget, despite relatively consistent rates of synthetic N input, implies that emission factors have high sensitivity to climate. The largest N_2O emissions were measured in 2012 (585 Gg N_2O-N·y^{-1}), which was characterized by the warmest mean annual air temperature (11.4 °C, +2.4 °C warmer than the climate normal) during our observations, and the warmest spring (March through May, 13.9 °C, +4.5 °C warmer than normal) in the last 122 y for the Corn Belt (14). Although 2012 was also one of the driest years on record (648 mm average, rank 10 of 122 y), the antecedent precipitation in the previous 2 y and during the winter months of 2011–2012 were above normal (32 mm to 130 mm above normal) (14), resulting in significant spring stream flow (*SI Appendix*, Fig. S8). Nitrous oxide emissions were remarkably consistent from 2013 to 2015, likely from compensating effects among environmental drivers. For instance, indirect emissions in June 2014 were significantly enhanced by precipitation, whereas direct emissions in June 2013 increased because of a combination of antecedent precipitation and relatively warm temperatures (*SI Appendix*, Fig. S9). Consideration of the N inputs to the system indicates a mean regional emission factor of 5.3 ± 1.2%, which is in good agreement with the global emission factor of 4% (3) that is based on top-down analyses. However, the emission factor reached a maximum of 7.5% in 2012, nearly double the previous estimates for this region (16, 20).

There are three modes of seasonal behavior (Fig. 2): spring thaw (DOY 50 to 120; February 19 to April 30); the priming of agricultural systems with spring N fertilizer and early season crop growth (DOY 135 to 200; May 15 to July 19); and episodic behavior in late fall and winter (DOY 300 to 365; October 27 to December 31) driven by fall application of N and freeze–thaw activity (21). Spring thaw has been recognized as a dominant control on the annual N_2O budget (21, 22) and is shown here to be a regional phenomenon concentrated within a 70-d window, typically initiated in mid-March. Considering the mean fluxes over the 6-y period (Fig. 1), spring thaw accounted for 30% of the annual budget, while the early growing season (May to July) accounted for about 53% of the annual emissions. Thus, over 80% of the annual N_2O emissions occurred within a period of about 150 d. The seasonality of the direct and indirect emissions was not in perfect phase. Indirect emissions have a more pronounced seasonal peak in May and June, which reflects the temporal dynamics and interaction of synthetic N application with runoff and stream flow within the region (15, 17). In the Corn Belt, most synthetic N fertilizer is applied in April (23), with peak tile flow and stream discharge occurring approximately April through June (24). Thus, the large total emission in 2012 was driven by large direct emissions in an exceptionally warm April followed by relatively large indirect emissions in May.

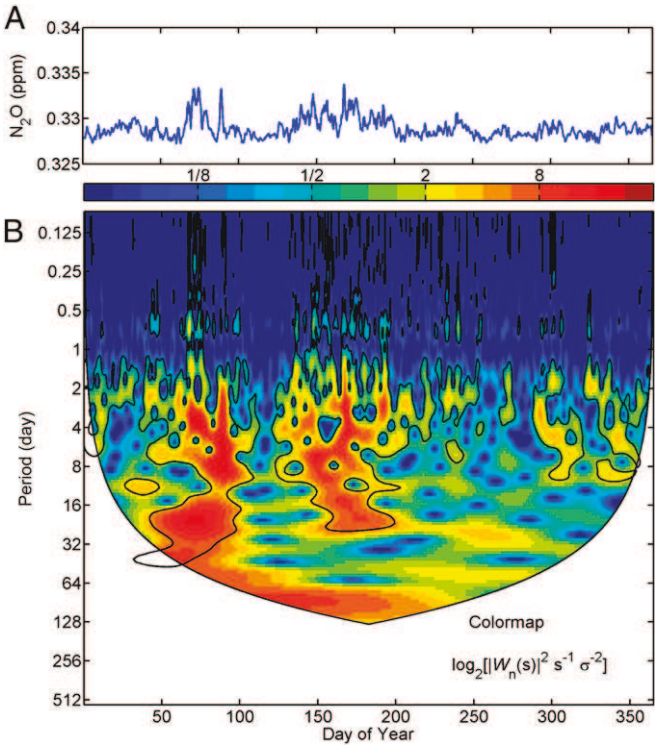

Fig. 2. Seasonal emission patterns and dominant modes of temporal variability in the tall tower N_2O mixing ratio observations extracted using wavelet techniques. (*A*) Ensemble (2010–2015) hourly average N_2O mixing ratios observed at the tall tower 100-m level. (*B*) Wavelet analysis of N_2O mixing ratios showing power in time-frequency space.

The sensitivity of N_2O emissions to climate drivers, including soil temperature and soil water content, has been studied under laboratory and field conditions (25–27), and these functions have been incorporated into land surface models such as the Community Land Model (CLM45-BGC-CROP). These empirical functions have been shown to have low statistical power under field conditions, a consequence of episodic behavior related to hot spots and hot moments (28). Tall tower mixing ratios and soil temperatures display moments of high correlation where the signals are in phase (*SI Appendix*, Fig. S10). We extracted periods of high wavelet coherence ($R^2 > 0.8$) from the multiyear time series to estimate the sensitivity of boundary layer N_2O mixing ratio to changes in air temperature and water-filled pore space (WFPS) (*SI Appendix*, Fig. S11 and Table S5). The linear sensitivity to air temperature during snow melt, growing season, and annually was 0.0488 parts per billion (ppb) per degree Celsius, 0.1710 ppb per degree Celsius, and 0.0404 ppb per degree Celsius , respectively. A nonlinear response in N_2O mixing ratios was observed at approximately −1.0 °C to 10.0 °C during spring thaw, corresponding to strong N_2O production near the 0 °C threshold and rapidly decreasing above 10 °C, presumably from increasing activity of N_2O reductase (29). Using this technique, the sensitivity of boundary layer N_2O mixing ratios to soil temperature was examined for conditions when WFPS limited N_2O production (26) (i.e., WFPS < 45%) and when it was near-optimal (i.e., 60% < WFPS <80%). These wavelet analyses revealed large differences in the planetary boundary layer N_2O mixing ratios, yielding temperature sensitivities of 0.0189 ppb per degree Celsius and 0.0583 ppb per degree Celsius, respectively. Similar wavelet analyses indicated weak but positive relationships between boundary layer N_2O mixing ratios and daily precipitation amount, indicating enhanced N_2O emissions for warmer and wetter climate conditions.

These sensitivity factors were applied to an equilibrium boundary layer budget analysis (16) to assess the potential impact of climate on the regional N_2O budget (Fig. 3). The 2010 equilibrium boundary layer budget of 420 Gg N_2O-N·y^{-1} (16) was similar to the mean emissions (411 Gg N_2O-N·y^{-1}) derived using the atmospheric inversions from 2010 to 2015 (Fig. 1) and is used here as a baseline value. The mean annual and spring temperature anomalies observed in 2012 demonstrate a change in the 2012 budget ranging from 20 Gg N_2O-N·y^{-1} to 120 Gg N_2O-N·y^{-1}, for the nonlimiting WFPS cases, giving an annual emission estimate ranging from 431 Gg N_2O-N·y^{-1} to 531 Gg N_2O-N y^{-1}. These equilibrium boundary layer budget analyses provide independent support for the Bayesian atmospheric inversion budget estimate of 585 Gg N_2O-N·y^{-1}. Further, these equilibrium boundary layer budget analyses indicate that the temperature sensitivity for the optimal WFPS function and the mean ensemble of the temperature sensitivity factors (Fig. 3*A*) yielded a Q_{10} temperature coefficient of 2.0. These regionally derived values are at the low end of reported Q_{10} values (2.1 to 8.1) based on flux chamber observations made in agricultural systems and laboratory microcosm experiments using agricultural soils (25–27).

We applied the mean ensemble of the nonlimiting WFPS air temperature sensitivity factors to the annual air temperature record for the US Corn Belt for the synthetic N intensive period (1970–2015) to examine perturbations in the regional N_2O budget and to identify possible trends over the past 46 y (Fig. 3*B*). Year-to-year fluctuations (peak-to-trough) are on the order of 65 Gg N_2O-N·y^{-1}, and there is a significant ($P = 0.023$) increasing trend of 1.7 Gg N_2O-N per decade (or about 7.6 Gg N_2O-N over the last 46 y) driven by increasing air temperature. These analyses imply that the interannual variability is large and that the change in N_2O emissions due to air temperature over this period is about 8% of that caused by the long-term trend of increasing synthetic N fertilizer use.

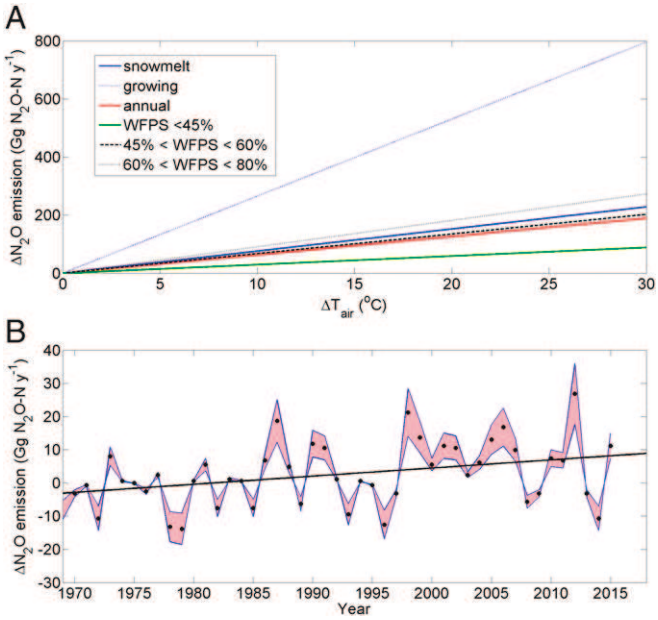

Fig. 3. Sensitivity of regional N_2O emissions to air temperate and WFPS derived from cross-wavelet coherence and equilibrium boundary layer budget analyses. (*A*) Sensitivity of the US Corn Belt N_2O budget to air temperature for different time periods and soil water content status. (*B*) Estimated perturbations in the US Corn Belt N_2O budget based on the long-term air temperature record of the Corn Belt and the ensemble of sensitivity factors shown in *A*. The shading represents 1 SD of the ensemble of sensitivity factors.

Simulations based on the biophysical model, CLM45-BGC-CROP, were used to help diagnose the sensitivity and feedback of the Corn Belt N_2O emissions to climate. Here, CLM45-BGC-CROP was modified to simulate direct and indirect emissions, and was optimized using the 2015 monthly emissions obtained from the inverse Bayesian analyses (Fig. 1) (*SI Appendix*, Fig. S12 and Tables S6 and S7). We then ran the model for the years 2010–2015 using this optimization. Because land use and synthetic N input were held constant in these simulations, the emission variability can be ascribed to variation in climate. The 2010–2015 simulations for direct (216.5 ± 42.4 Gg N_2O-N·y^{-1}), indirect (199.0 ± 57.0 Gg N_2O-N·y^{-1}), and total (415.5 ± 90.8 g N_2O-N·y^{-1}) emissions showed very good agreement with the Bayesian estimates. Model and observational constraints of the climate sensitivity showed good agreement. The CLM45-BGC-CROP Q_{10} temperature coefficient ranged from 1.1 to 1.6, depending on the WFPS, and was in good agreement with that derived from the tall tower wavelet analyses. The simulated emissions and observations were highly correlated over the 6-y period ($R^2 = 0.86$, $P = 0.0062$) and support that emissions in 2012 were anomalously large due to the extremely warm spring.

The model was run forward in time to 2050 using the Coupled Model Intercomparison Project Phase 5 (CMIP5) [scenario RCP8.5 (representative concentration pathway of +8.5 watts per square meter radiative forcing by the year 2100)] forcing data, while holding land use and synthetic N fertilizer input constant. For this long-term simulation, CLM45-BGC-CROP was reoptimized using all of the available emission data from the tall tower Bayesian analyses. Fig. 4 shows a general increasing trend in indirect (+0.87 Gg N_2O-N·y^{-1}, $P = 0.004$), direct (+0.13 Gg N_2O-N·y^{-1}, $P = 0.81$), and total (+1.0 Gg N_2O-N·y^{-1}, $P = 0.17$) N_2O emissions driven by climate, with an increasing trend in annual air temperature (0.038 °C·y^{-1}, $P < 0.001$) and precipitation (2.7 mm·y^{-1}, $P < 0.001$) for the US Corn Belt. The dominant driver of the increased annual emissions is the link between increasing

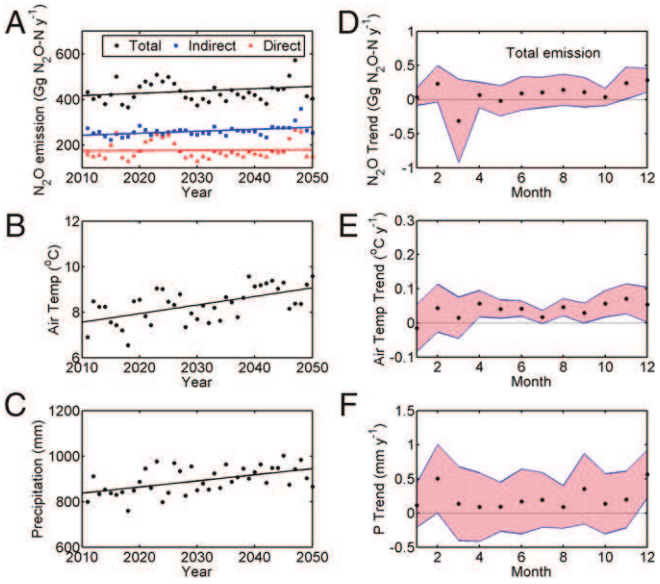

Fig. 4. Simulation of N_2O emissions using CLM45-BGC-CROP for the US Corn Belt from 2011 to 2050. Simulations were performed using the CMIP5 (scenario RCP8.5) forcing data, while holding land use and synthetic N fertilizer input constant. (*A*) Trend in the annual total, indirect, and direct N_2O emissions. (*B*) Trend in annual air temperature. (*C*) Trend in annual precipitation. (*D*) Monthly trend in total N_2O emissions. (*E*) Monthly trend in air temperature. (*F*) Monthly trend in precipitation. In *D*–*F*, the shading indicates the 95% confidence intervals.

precipitation and indirect emissions. The seasonal variability indicates that substantially warmer temperatures in April and wetter antecedent conditions in spring (i.e., increased wintertime precipitation in December and February) are important drivers of the increasing spring runoff (*SI Appendix*, Fig. S13) and emissions. However, there is also an increase in summer and late fall emissions. Considering the individual trends in synthetic N application (*SI Appendix*, Fig. S1) and climate suggests that emissions could increase from the Corn Belt by about 200 Gg N_2O-N, with total average emissions exceeding 600 Gg N_2O-N by 2050. These model results indicate that the long-term increase in N_2O emissions due to climate change is about 25%. Thus, using two different constraints (modeling and planetary boundary layer observations and sensitivity analyses), we found that the climate sensitivity of N_2O emissions accounts for about 8 to 25% of the long-term trend.

Although the long-term N_2O emission trends are derived primarily from the increased use of synthetic N (3, 7, 11), the large observed interannual variability of N_2O emissions and the model-simulated trends support that positive feedbacks associated with climate change will be important. These temporal dynamics pose a major challenge to mitigation efforts and emissions accounting. Indeed, Davidson (30) has shown that a 50% reduction in N_2O emission factors and per capita meat consumption would be required to stabilize emissions within representative concentration pathways outlined in the fifth assessment of the Intergovernmental Panel on Climate Change. The positive climate feedback effect implies that even greater reductions in synthetic N application or increased nitrogen use efficiency (6) will be required to balance emission budgets as outlined in the Paris Agreement. Such reductions will be difficult to achieve given the increasing demand for food, fiber, and biofuel (6, 7), and the fact that grain yields are likely to decline with increasing air temperatures (31). Increasing runoff and N leaching due to increased precipitation are likely to exacerbate the situation (17). Finally, evidence is emerging that mitigation strategies related to N fertilizer management, e.g., delaying the timing of fertilizer application (32), or using microbial inhibitors (33, 34), are made less reliable under warmer, wetter, and more variable climate. However, we cannot rule out that warmer and wetter conditions could benefit other mitigation options such as the use of winter cover crops (35) or perennial companion crop systems (36). Here, the growth of cover crops in early spring could reduce the available soil nitrate and reduce N_2O emissions. Results from these cover crop studies, however, have produced inconsistent results. The potential impact of climate change on N_2O mitigation strategies remains speculative, and requires further research.

Materials and Methods

Tall Tower Observations. Tall tower N_2O mixing ratios were measured at the Minnesota Public Radio communications tower, KCMP (44° 41′ 19″ N, 93° 4′ 22″ W; 290 m above sea level), using a tunable diode laser technique (TGA100; Campbell Scientific Inc.) at four heights including 32, 56, 100, and 185 m above the ground (16). These measurements were initiated in April 2010 and are on-going as of September 2017. Calibrations were performed hourly with gases traceable to the National Oceanic and Atmospheric Administration–Earth System Research Laboratory (NOAA-ESRL) 2006A N_2O mole fraction scale. Details regarding calibration and data filtering are provided in *SI Appendix*.

Inverse Modeling. The atmospheric inverse modeling approach used in this study is based on Chen et al. (15), who partitioned regional N_2O emissions from the US Corn Belt into direct and indirect emissions. A scale factor Bayesian inverse (SFBI) method was applied for each month (April to October from 2010 through to 2015). Briefly, this methodology consists of the following key steps: (*i*) The tall tower concentration footprints for the 100-m air sample level (receptor) were estimated for each hour using the Stochastic Time-Inverted Lagrangian Transport (STILT) model. The Weather Research and Forecasting model (version 3.5.1) provided input to STILT, including wind conditions, atmospheric stability, and planetary boundary layer height. (*ii*) The tall tower concentration footprints were multiplied by the a priori emission estimates to obtain an initial guess of the N_2O mixing ratio enhancement at the tall tower receptor. The a priori emissions were obtained from the Emission Database for Global Atmospheric Research (EDGAR) 4.2 and EDGAR2.0 databases; CLM45-BGC-CROP model, Global Fire Emissions Database (version 3, 2011, www.globalfiredata.org), and the upscaling of observations of indirect N_2O emissions from rivers and streams (17). (*iii*) The estimate of the tall tower N_2O mixing ratio enhancement was then added to the background N_2O mixing ratio. Background N_2O mixing ratios were estimated based on observations from the NOAA Carbon Cycle and Greenhouse Gases program (37) and were obtained at the outer edge of the concentration source footprint. (*iv*) Finally, the SFBI was used to optimize the a priori emissions along with the relative contributions of the direct and indirect emissions. A detailed description of the SFBI is provided in *SI Appendix*, and the sensitivity of the inversion results to a priori source types, tall tower data quality, tall tower data filtering, a priori emission errors, and a priori indirect emission source estimates are provided in *SI Appendix*, Tables S1–S4. Note that the partitioning of total N_2O emissions into indirect and direct emissions is sensitive to the prescribed uncertainties of the a priori emissions. For instance, the average (for years 2010–2015) indirect emissions varied from 154.5 Gg N_2O-N·y^{-1} to 200.2 Gg N_2O-N·y^{-1} for a 200 to 400% change in the a priori uncertainty when the direct emission a priori uncertainty was fixed at a nominal value of 66% (*SI Appendix*, Table S3).

Wavelet Analyses. Nitrous oxide mixing ratios and associated environmental variables were analyzed using techniques based on the continuous wavelet transform (CWT). All CWTs were calculated on the fluctuating component of the signal using the complex Morlet wavelet basis with the nondimensional frequency (ω_0) set to 6 (38). Scales were set to have a minimum of 2 h (i.e., twice the hourly averaging interval), and to have 12 suboctaves per octave. Calculating the CWT of the signal yields a set of wavelet coefficients, $W_n(s)$, spanning all times (n) and scales. We examined the relation between N_2O mixing ratios in the planetary boundary layer (PBL) and environmental drivers by applying the multivariate technique known as wavelet coherence analysis to identify correlation and phase relationships among variables (39). Here, we applied a diurnal filter (24-h running mean) to the N_2O mixing ratio data to reduce the effects of diurnal PBL growth dynamics on the variations of N_2O. We used a minimum coherence threshold ($R^2 = 0.80$) to select relationships among environmental factors. Linear regression was then used to quantify these relationships and estimate climate sensitivity factors. See *SI Appendix* for further details.

Boundary Layer Budget Sensitivity. We used the equilibrium boundary layer budget theory as a framework to help diagnose how observed changes in temperature and WFPS influence the N_2O budget as

$$F_{EBL} = \int_0^h \rho \frac{dc}{dt} dh + S(C_t - C_m), \quad [1]$$

where F_{EBL} is the surface flux, S represents the subsidence of air from the free troposphere into the boundary layer (units of moles per square meter per second and positive toward the surface), and C_t and C_m represent the mixing ratios of N_2O in the free atmosphere and mixed layer, respectively. For the sensitivity analyses shown in Fig. 3, we use the values of S and C_t for 2010 (16) with $C_m = C_t + C_m(T)$. Here, $C_m(T)$ represents the air temperature sensitivity factors shown in *SI Appendix*, Fig. S11.

Land Surface Model Projections. The CLM45-BGC-CROP model was modified to simulate direct N_2O emissions based on previously published algorithms (40, 41), with indirect emissions constrained using model estimates of nitrate runoff/leaching and applying the most recent estimates of the runoff/leaching emission factors for the Corn Belt region (15). The model was then optimized using the 2015 monthly Bayesian N_2O emissions by adjusting the timing and amount of fertilizer applied to croplands and by adjusting the model's nitrification parameters (i.e., the maximum fraction of NH_4^+ nitrified per day) (*SI Appendix*, Fig. S12 and Tables S6 and S7). CLM45-BGC-CROP was run for 40 y (2011–2050), forced with atmospheric data from CMIP5 (42). The forcing data were simulated using a global climate model developed by the Meteorological Research Institute (MRI), MRI-CGCM3 (43). The CMIP5 simulations represent the RCP8.5 scenario run for years 2006–2080 with a spatial resolution of 1.125° × 1.125°. In the model, 3-hourly air temperature, wind, incident solar radiation, precipitation, and specific humidity were used to drive CLM45-BGC-CROP.

ACKNOWLEDGMENTS. This research was partially supported by the US Department of Agriculture (USDA) (Grant 2013-67019-21364), USDA Agricultural Research Service, NOAA (Grant NA13OAR4310086), US National Science Foundation (Grant 1640337), Minnesota Corn Growers Association (Grant 4118-15SP), and the Minnesota Supercomputing Institute for Advanced Computational Research (https://www.msi.umn.edu/). We acknowledge the support of an MnDrive PhD fellowship (to Z.C.).

1. Food and Agricultural Organization of the United Nations (2015) *World Fertilizer Trends and Outlook to 2018*. Available at www.fao.org/3/a-i4324e.pdf. Accessed February 3, 2017.
2. Erisman JW, et al. (2008) How a century of ammonia synthesis changed the world. *Nat Geosci* 1:636–639.
3. Crutzen PJ, Mosier AR, Smith KA, Winiwarter W (2008) N_2O release from agro-biofuel production negates global warming reduction by replacing fossil fuel. *Atmos Chem Phys* 8:389–395.
4. Montzka SA, Dlugokencky EJ, Butler JH (2011) Non-CO_2 greenhouse gases and climate change. *Nature* 476:43–50.
5. Ravishankara AR, Daniel JS, Portmann RW (2009) Nitrous oxide (N_2O): The dominant ozone-depleting substance emitted in the 21st century. *Science* 326:123–125.
6. Zhang X, et al. (2015) Managing nitrogen for sustainable development. *Nature* 528: 51–59.
7. Galloway JN, et al. (2008) Transformation of the nitrogen cycle: Recent trends, questions, and potential solutions. *Science* 320:889–892.
8. International Plant Nutrition Institute (IPNI) (2012) A Nutrient Use Information Systems (NuGIS) for the U.S, Available at www.ipni.net/nugis. Accessed February 3, 2017.
9. Davidson EA (2009) The contribution of manure and fertilizer nitrogen to atmospheric nitrous oxide since 1860. *Nat Geosci* 2:659–662.
10. Ciais, et al. (2013) *Climate Change 2013: The Physical Science Basis. Contribution of Working Group 1 to the Fifth Assessment Report of the Intergovernmental Panel on Climate Change*, eds Stocker TF, et al. (Cambridge Univ Press, Cambridge, UK).
11. Reay DS, et al. (2012) Global agriculture and nitrous oxide emissions. *Nat Clim Change* 2:410–416.
12. Trenberth KE (2011) Changes in precipitation with climate change. *Clim Res* 47:123–138.
13. Butterbach-Bahl K, Baggs EM, Dannenmann M, Kiese R, Zechmeister-Boltenstern S (2013) Nitrous oxide emissions from soils: How well do we understand the processes and their controls? *Philos Trans R Soc Lond B Biol Sci* 368:20130122.
14. NOAA National Centers for Environmental information (2016) Climate at a Glance: U.S. Available at www.ncdc.noaa.gov/cag/. Accessed August 1, 2016.
15. Chen Z, et al. (2016) Partitioning N_2O emissions within the US Corn Belt using an inverse modeling approach. *Global Biogeochem Cycles* 30:1192–1205.
16. Griffis TJ, et al. (2013) Reconciling the differences between top-down and bottom-up estimates of nitrous oxide emissions for the US Corn Belt. *Global Biogeochem Cycles* 27:746–754.
17. Turner PA, et al. (2015) Indirect nitrous oxide emissions from streams within the US Corn Belt scale with stream order. *Proc Natl Acad Sci USA* 112:9839–9843.
18. Donner SD, Scavia D (2007) How climate controls the flux of nitrogen by the Mississippi River and the development of hypoxia in the Gulf of Mexico. *Limnol Oceanogr* 52:856–861.
19. Turner PA, et al. (2016) Regional-scale controls on dissolved nitrous oxide in the Upper Mississippi River. *Geophys Res Lett* 43:4400–4407.
20. Miller SM, et al. (2012) Regional sources of nitrous oxide over the United States: Seasonal variation and spatial distribution. *J Geophys Res Atmos* 117:D06310.
21. Wagner-Riddle C, Thurtell GW (1998) Nitrous oxide emissions from agricultural fields during winter and spring thaw as affected by management practices. *Nutr Cycl Agroecosyst* 52:151–163.
22. Wagner-Riddle C, et al. (2017) Globally important nitrous oxide emissions from croplands induced by freeze-thaw cycles. *Nat Geosci* 10:279–283.
23. Wade T, Claassen R, Wallander S (2015) Conservation-practice adoption rates vary widely by crop and region. (US Dept of Agriculture, Economic Research Service, Washington, DC), Economic Information Bulletin 147.
24. United States Geological Survey (2017) *Current Water Data for Minnesota*. Available at waterdata.usgs.gov/mn/nwis/rt. Accessed July 13, 2017.
25. Smith KA, et al. (1998) Effects of temperature, water content and nitrogen fertilization on emissions of nitrous oxide by soils. *Atmos Environ* 32:3301–3309.
26. Dobbie KE, et al. (1999) Nitrous oxide emissions from intensive agricultural systems: Variations between crops and seasons, key driving variables, and mean emission factors. *J Geophys Res Atmos* 104:26891–26899.
27. Venterea RT (2007) Nitrite-driven nitrous oxide production under aerobic soil conditions: Kinetics and biochemical controls. *Glob Change Biol* 13:1798–1809.
28. Groffman PM, et al. (2009) Challenges to incorporating spatially and temporally explicit phenomena (hotspots and hot moments) in denitrification models. *Biochemistry* 93:49–77.
29. Muller C, Kammann C, Ottow JCG, Jager HJ (2003) Nitrous oxide emission from frozen grassland soil and during thawing periods. *J Plant Nutr Soil Sci* 166:46–53.
30. Davidson EA (2012) Representative concentration pathways and mitigation scenarios for nitrous oxide. *Environ Res Lett* 7:024005.
31. Lobell DB, et al. (2013) The critical role of extreme heat for maize production in the United States. *Nat Clim Change* 3:497–501.
32. Venterea RT, Coulter JA (2015) Split application of urea does not decrease and may increase N_2O emissions in rainfed corn. *Agron J* 107:337–348.
33. Parkin TB, Hatfield JL (2014) Enhanced efficiency of fertilizers: Effect on nitrous oxide emissions in Iowa. *Agron J* 106:694–702.
34. Sistani KR, Jn-Baptiste M, Lovanh N, Cook KL (2011) Atmospheric emissions of nitrous oxide, methane, and carbon dioxide from different nitrogen fertilizers. *J Environ Qual* 40:1797–1805.
35. Basche AD, Miguez FE, Kaspar TC, Castellano MJ (2014) Do cover crops increase or decrease nitrous oxide emissions? A meta-analysis. *J Soil Water Conserv* 69:471–482.
36. Turner PA, Baker JM, Griffis TJ, Venterea RT (2016) Impact of kura clover living mulch on nitrous oxide emissions in a corn-soybean system. *J Environ Qual* 45:1782–1787.
37. Dlugokencky EJ, Steele LP, Lang PM, Masarie KA (1994) The growth rate and distribution of atmospheric methane. *J Geophys Res* 99:17021–17043.
38. Torrence C, Compo GP (1998) A practical guide to wavelet analysis. *Bull Am Meteorol Soc* 79:61–78.
39. Grinsted A, Moore J, Jevrejeva S (2004) Application of the cross wavelet transform and wavelet coherence to geophysical time series. *Nonlinear Process Geophys* 11: 561–566.
40. Del Grosso SJ, et al. (2000) General model for N_2O and N_2 gas emissions from soils when comparing observed and gas emissions rates from irrigated field soils used for model testing NO_2.. *Global Biogeochem Cycles* 14:1045–1060.
41. Parton W, et al. (2001) Generalized model for NO_x and N_2O emissions from soils. *J Geophys Res* 106:17403–17419.
42. Taylor KE, Stouffer RJ, Meehl GA (2012) An overview of CMIP5 and the experiment design. *Bull Am Meteorol Soc* 93:485–498.
43. Yukimoto S, et al. (2012) A new global climate model of the Meteorological Research Institute: MRI-CGCM3–model description and basic performance. *J Meteorol Soc Japan* 90A:23–64.